The effects of composition, temperature and hydrostatic pressure on phase transition behaviors in $(Pb_{1-1.5x}La_x)(Zr_{0.8}Ti_{0.2})O_3$ ceramics

Meng Xie (xiemeng19@mails.ucas.ac.cn)
Shanghai Institute of Ceramics Chinese Academy of Sciences https://orcid.org/0000-0002-6612-903X
Yizheng Bao
Shanghai Institute of Materia Medica Chinese Academy of Sciences
Hengchang Nie
Shanghai Institute of Ceramics Chinese Academy of Sciences
Fei Cao
Shanghai Institute of Ceramics Chinese Academy of Sciences
Xianlin Dong
Shanghai Institute of Ceramics Chinese Academy of Sciences
Genshui Wang
Shanghai Institute of Ceramics Chinese Academy of Sciences

Research Article

Keywords: Phase transition, PLZT, ferroelectrics, anti-ferroelectrics

Posted Date: May 6th, 2020

DOI: https://doi.org/10.21203/rs.3.rs-25916/v1

Abstract

In this work, $(Pb_{1-1.5x}La_x)(Zr_{0.80}Ti_{0.20})O_3$ (abbreviated as PLZT, x = 0.01, 0.03, 0.04, 0.06, 0.07) ceramics are designed on the base of chemical composition modification and prepared by solid-state reaction. The effect of composition, temperature, and hydrostatic pressure on ferroelectric-antiferroelectric (FE-AFE) phase transition is investigated. It is obtained that phase transition from ferroelectric rhombohedral phase to antiferroelectric tetragonal phase as a function of La^{3+} doping content, especially, the PLZT ceramics of x = 0.04, 0.06, and 0.07 are the coexistence of FE-AFE phase. It is also found the FE-AFE phase transition driven by increased temperature in poled PLZT ceramics (x = 0.04, 0.06). Furthermore, static charges density (P_r) of PLZT (x = 0.04, 0.06) are decreased from 29.11 μC/cm^2 and 31.52 μC/cm^2 to 19.76 {\mu }C/cm^2, 6.45 {\mu }C/cm^2 under 400 MPa hydrostatic pressure due to the pressure-induced FE-AFE phase transition. The depolarization rates are 32.12% and 79.54%, respectively. Meanwhile, the phase diagram of $(Pb_{1-1.5x}La_x)(Zr_{0.80}Ti_{0.20})O_3$ ceramics is acquired roughly. These results provide guidance for the engineering application of $(Pb_{1-1.5x}La_x)(Zr_{0.80}Ti_{0.20})O_3$ ceramics.

1. Introduction

Ferroelectric (FE) lead-containing materials with spontaneous polarization, is the significant functional materials and has been studied for many years [1]. Lead zirconate titanate ($Pb(Zr,Ti)O_3$, (PZT)) ceramics with outstanding piezoelectric and ferroelectric properties are representative compositional system for ferroelectric materials, widely utilized in modern ferroelectric transducers, sensor, actuators and ultrahigh-power system [2–6].

Based on reported studies, modification with dopants has been an acknowledged and effective approach to optimize the performance of PZT ceramics [7–12]. In particular, compositions near phase boundary have been concentrated on more interest over the past few decades, because of that phase transition of polar state and nonpolar state involving to the generation/release electric polarization have a wide range of applications [7, 13–15]. $Pb(Zr,Sn,Ti)O_3$, $(Pb,Nb)(Zr,Sn,Ti)O_3$, and $(Pb,La)(Zr,Sn,Ti)O_3$ ceramics obtained through modification of PZT ceramics with Sn and La are all promising ferroelectric materials, extensively studied and applied [7, 8, 16].

In addition, $(Pb,La)(Zr,Ti)O_3$ (PLZT) ceramics acquired through modification of PZT ceramics with lanthanum (La) are also representative ferroelectric materials [17–22]. The coupling of ferroelectric reactive oxygen octahedrons broken by the replacement of La^{3+}(1.36 Å) for Pb^{2+} (1.49 Å) at A-sites give rise to phase transformation[19, 23]. In particular, the excellent piezoelectricity, pyroelectricity and energy-storage properties are possessed by compositions located in phased boundary [19, 24–28]. For example, Ciuchi et al. investigated the energy storage performances of $(Pb_{1-x}La_x)(Zr_{0.90}Ti_{0.10})_{1-x/4}O_3$ ceramics with La compositions near the FE-AFE phase boundary [26]. Qiao et al. reported the effect of FE-AFE phase transition on enhanced pyroelectric properties in $(Pb_{1-1.5x}La_x)$ $(Zr_{0.86}Ti_{0.14})$ O_3 ceramics [27]. Besides, high piezoelectricity of PLZT ceramics near phase boundary was evident by Kumar et al [28]. In

general, it's fundamental and significant to investigate the phase transition in PLZT ceramics for application. However, to date, there were rare attentions paid to the effect of composition, temperature, especially, hydrostatic pressure on FE-AFE phase transition in $(Pb_{1-1.5x}La_x)(Zr_{0.80}Ti_{0.20})O_3$.

In this paper, the effect of composition, temperature, and hydrostatic pressure on phase transition behaviors in $(Pb_{1-1.5x}La_x)(Zr_{0.80}Ti_{0.20})O_3$ (x = 0.01, 0.03, 0.04, 0.06, 0.07) ceramics are investigated thoroughly. XRD patterns, temperature-dependent *P-E* hysteresis loops, and temperature-dependent dielectric constant curve demonstrate phase transition between FE_R and AFE_T driven by increased La content and temperature. What's more, the depolarization behaviors of poled PLZT(x = 0.04, 0.06) under hydrostatic pressure are investigated. These results indicate La doping at A-sites reconfigures the phase boundary of FE state and AFE state in PLZT ceramics. Besides, it also unveil the FE-AFE phase transition of $(Pb_{1-1.5x}La_x)(Zr_{0.80}Ti_{0.20})O_3$ ceramics for promising potential engineering applications.

2. Experimental Procedure

$(Pb_{1-1.5x}La_x)(Zr_{0.8}Ti_{0.2})O_3$ (x = 0.01, 0.03, 0.04, 0.06, 0.07) ceramics were prepared via conventional solid reaction method. Raw materials were reagent-grade metal oxides Pb_3O_4 (99.5%), La_2O_3 (99.95%), ZrO_2 (99.99%), TiO_2 (99.21%). 0.5 mol% additional Pb_3O_4 were added in order to compensate Pb volatilization during sintering. The powders were weighted according to the stoichiometric composition and ball milled 12 h in Teflon jars with deionized water and zirconium ball as media. After drying, the powders were calcined at 925℃ for 2 h. And the calcined powders were ball milled again for 24 h. The polyvinyl alcohol (PVA), a binder for granulation, was mixed into calcined powders. The powders were pressed into pellets with 13 mm diameter. After burning off PVA, the pellets buried with same composition to minimize Pb volatilization in alumina crucible, were sintered at 1300 ℃ for 2 h with a heating rate of 2 ℃/min. The sintered pellets were polished to a thickness of 0.5 mm and both sides of samples were covered with fired-on silver paste, calcined at 600℃ for 2 h.

Crystal structure was studied by using X-ray diffraction (XRD, D/MAX-2550V; Rigaku, Tokyo, Japan). Cross-sectional microstructure was observed using a TM 3000 Tabletop Microscope (Hitachi, Tokyo, Japan). The dielectric constant (ϵ_r) and tangent loss ($tan\delta$) were tested by using a LCR meter (Model E4980; Agilent, Palo Alto, CA, USA). Polarization-electric field (*P-E*) hysteresis loops and depolarization behaviors under hydrostatic pressure were measured using an aixACCT TF 2000 Analyzer FE measuring by system (aix ACCT Co., Aachen, Germany) with home-made hydrostatic loading apparatus [29].

3. Result And Discussion

3.1 Structure properties

As shown in Fig. 1, the perovskite structure with second phases PbO_2 (PDF#50-1430) is observed in the XRD patterns of PLZT ceramics. The peak is shifted slightly to higher 2θ with the increased La content,

indicating decrease of lattice constant and smaller unit cell volume, attributed to oxygen octahedral distortion causing by the replacement of La^{3+}(1.36 Å) for Pb^{2+} (1.49 Å) at A-sites. Detailed XRD patterns in 2θ plotted in Fig. 1b and Fig. 1c, it can be observed the peak splitting in the (111) reflections in the PLZT ceramics of x = 0.01, 0.03, indicating a predominantly rhombohedral distortion, that is, the nature of FE_R phase. With increased La content (x = 0.04, 0.06, 0.07), the peak splitting are observed in the (200) reflections and the (111) reflections are gradually transformed to single peak, indicating the phase switching to tetragonal distortion, that is, the coexistence of FE_R phase and AFE_T phase [30]. The result reveals that the occurrence of FE_R-AFE_T phase transition is driven by increased La content.

The cross-sectional SEM images of fresh samples sintered at 1300 °C are shown in Fig. 2. With increased La content, the grain size is decreased significantly. In addition, these cross-sections are fractured along intergranular direction under external force when La content x = 0.01, 0.03 and 0.04; whereas cross-sections for x = 0.06 and 0.07 are fractured along trans-granular direction under external force.

3.2 Dielectric properties

Temperature-dependent relative dielectric constant (ϵ_r) and dielectric loss ($tan\delta$) of PLZT ceramics as a function of temperature at different frequencies are displayed in Fig. 3a-e. Similar temperature-dependent behavior at the Curie temperature(T_C) are obsevered in the samples of x = 0.01 and 0.03. T_C is defined by the temperature of the maximum dielectric constent, regarded as a thermodynamic scale for the transition energy barrier from the FE or AFE phase to paraelectric (PE) phase. [31] While two dielectric anomalies can be observed in the PLZT ceramics of x = 0.04 and 0.06: T_{FE-AFE} and T_C. T_{FE-AFE} can be determined by the first dielectric constant inflection point and dielectric loss peak, attributed to the transformation from FE to AFE. Hence, T_{FE-AFE} has also been regared as the depolarization temperature (T_d) of the sample. As for the sample with x = 0.07, it can be only seen phase transition from AFE to PE since the AFE phase is dominanted. In Fig. 3f, the T_C corresponding to the samples of x = 0.01, 0.03, 0.04, 0.06, 0.07 are 240℃, 207℃, 143℃, 128℃, 114℃, respectively. Furthermore, ϵ_{max} is decreased from 42025 to 5435 with increased La content, and the $tan\delta$ is less than 0.083. Therefore, it is confirmed that the PLZT ceramics of x = 0.04, 0.06 are lying around the FE-AFE phase boundaries and experience FE-AFE phase transition near 125℃ and 80℃, while the PLZT ceramics of x = 0.01, 0.03 are stable FE_R before T_C.

3.3 Ferroelectric properties

The *P-E* hysteresis loops of all as-sintered specimens from 30℃ to 170℃ can be observed in Fig. 4 to further confirmed temperature-induced phase transition shown in Fig. 3. As shown in Fig. 4a, b, well-shaped *P-E* hysteresis loops show that these components are stable FE_R independent of temperature, where 170℃ is less than T_C shown in Fig. 3a and b. PLZT ceramics of x = 0.04, 0.06 are transformed from well-shaped *P-E* loops to double hysteresis loops and then to slim P-E loops, indicating transition of FE phase to AFE phase and then to PE phase [32, 33]. Phase transformation from AFE to PE with La

content x = 0.07 is exhibited in Fig. 4e. Moreover, the phase transition temperature is decreased from about 130 ℃ to 90 ℃ with increased La content corresponding to Fig. 3f, in which defects produced by the aliovalent substitution and the long range order of ferroelectric domains destroyed are beneficial to the inversion of domain wall [34]. P_r and coercive field E_C are decreased remarkably and the loops are much slimmer with further increased temperature and La content [1]. In the Fig. 4f and Fig. 3f, it can be observed excellent temperature stability for P_r of samples of x = 0.01, 0.03; while there is a sharp decrease in P_r for samples of x = 0.04, 0.06, proving temperature dominates FE-AFE transition. In a way, there is temperature-induced structural phase transition and depolarization behaviors in the PLZT ceramics of x = 0.04 and 0.06.

3.4 Depolarization under hydrostatic pressure

PLZT(x = 0.04, 0.06) ceramics with higher P_r and near the phase boundary between FE and AFE phase are chosen to study the depolarization under hydrostatic pressure. These samples were polarized at 2.0 kV/mm for 15 min at room temperature in an silicone oil bath, and then placed for 24 h after polarization to obtain stable P_r. *P-E* hysteresis loops and *I-E* loops of PLZT(x = 0.04, 0.06) ceramics at electric field of 4 kV/mm and under the hydrostatic pressure increasing from 0 MPa to 400 MPa are shown in Fig. 5. Well-shaped P-E hysteresis loops with the P_r decreased from 29.11 μC/cm^2 to 19.76 μC/cm^2 are shown in Fig. 5(a1). It's also observed that the maximum pressure used in the experiment do not reach the critical depolarization pressure. What's more, E_C is decreased from 1.09 to 0.94 kV/mm with increased pressure to 400 MPa, indicating that a predominant FE ordering gradually decreases. As shown in Fig. 5(a2), with increased hydrostatic pressure, the current peak gradually slows down and the polarization is gradually released in the form of current under additional field. Clearly, the P_r of sample x = 0.06 is decreased from 31.52 μC/cm^2 to 6.45 μC/cm^2, as shown in the Fig. 5(b1). It's exhibited in Fig. 5(b2) that the single current peak is transformed to double current peak with the transition from FE_R phase to AFE_T phase under the effect of hydrostatic pressure, which is similar to temperature-induced phase transition shown in Fig. 3 and Fig. 4. According to soft mode theory, hydrostatic pressure with spherical symmetry increases the interactions between adjacent cations and anions more rapidly than it increases long-range Coulomb forces, increasing the AFE phase stability, and releasing stored charges in a very short period of time [30].

To further evaluate pressure-induced depolarization behaviors, the remnant polarization of poled PLZT (x = 0.04, 0.06) are shown in Fig. 6(a). It can be observed that the P_r of x = 0.04 is decreased steadily under hydrostatic pressure, and the P_r of x = 0.06 is decreased rapidly after hydrostatic pressure of 250 MPa. Meanwhile, the remnant polarizations are decreased from P_{r1} = 29.11 μC/cm^2, 31.52 μC/cm^2 to P_{r2} = 19.76 μC/cm^2, 6.45 μC/cm^2, respectively, with depolarization rates of 32.12% and 79.54%,calculated by (see Equation 1 in the Supplementary Files) $R_T = -\frac{P_{r2}-P_{r1}}{P_{r1}} \times 100\%$ under 400 MPa pressure. These results demonstrate that the oriented FE domains are rearranged under the influence of hydrostatic

pressure, accompanied by irreversible FE-AFE phase transition and the release of polarization. The results also demonstrate the promising potential application of $(Pb_{1-1.5x}La_x)(Zr_{0.8}Ti_{0.2})O_3$ ceramics in pulsed power supply.

Based on the above results, a simple phase diagram of $(Pb_{1-1.5x}La_x)(Zr_{0.8}Ti_{0.2})O_3$ ceramics is proposed. The phase diagram of PLZT ceramics for x = 0.01, 0.03, 0.04, 0.06, 0.07 are summarized in Fig. 6(b), determined by the temperature of T_C corresponding to the maximum values of dielectric constant and dielectric loss in the Fig. 3, employed to classify the boundary of FE and PE phase. The AFE phase can be stabilized by doping La^{3+} and destabilized by Ti^{4+} doping [5], so that PLZT ceramics are transformed from FE to AFE phase with La doping, manifesting AFE phase tends to be stable and a FE-AFE phase boundary is constructed by La in PLZT-based ceramics [35, 36].

4. Conclusion

In summary, the effect of composition, temperature and hydrostatic pressure on phase transition behaviors in $(Pb_{1-1.5x}La_x)(Zr_{0.80}Ti_{0.20})O_3$ ceramics were investigated thoroughly, with emphasis on ferroelectric, dielectric performances, and depolarization behaviors. With increased La content, PLZT (x = 0.01, 0.03, 0.04, 0.06, 0.07) ceramics underwent transition from FE_R phase to AFE_T phase. Aliovalent A-site substitution of La^{3+} doping interrupted long-range ordered ferroelectric domains, driving FE_R-AFE_T phase switching. The lattice constant was decreased and the peak value was shifted to higher 2θ as a whole. Temperature-dependent P-E hysteresis loops and temperature-dependent relative dielectric constant (ϵ_r) and dielectric loss ($tan\delta$) demonstrated PLZT(x = 0.01, 0.03) ceramics were stable FE_R phase, while PLZT(x = 0.04, 0.06, 0.07) coexisted FE phase and AFE phase. With the increase of temperature, the domains overcame the energy barrier to achieve FE-AFE phase transition. There was thermal-induced FE-AFE phase transition and depolarization behaviors in the PLZT ceramics of x = 0.04, 0.06. Pressure-dependent P-E loops and I-E loops illustrated the polarized sample PLZT (x = 0.04, 0.06) ceramic could be depolarized with depolarization rate of 38.51% and 79.54%, respectively. According to the effect of external field on FE-AFE phase transition, it indicated that $(Pb_{1-1.5x}La_x)(Zr_{0.8}Ti_{0.2})O_3$ ceramics had promising potential in the field engineering application.

Declarations

Acknowledgements

This work was supported by National Natural Science Foundation of China (Grant No. 11774366, 51872312), Youth Innovation Promotion Association, CAS (Grant No. 2017296), and Natural Science Foundation of Shanghai (Grant NO.18ZR1444900).

References

[1] Haertling G H. Ferroelectric ceramics: History and technology. *J Am Ceram Soc* 1999, **82**: 797-818.

[2] Jaffe B, Roth R S, Marzullo S. Piezoelectric properties of lead zirconate-lead titanate solid-solution ceramics. *J Appl Phys* 1954, **25**: 809-810.

[3] Zeng T, Dong X L, Mao C L, *et al*. Effects of pore shape and porosity on the properties of porous PZT 95/5 ceramics. *J Eur Ceram Soc* 2007, **27**: 2025-2029.

[4] Xu Y. Ferroelectric materials and their applications, Elsevier, 2013.

[5] Hao X, Zhai J, Kong L B, *et al*. A comprehensive review on the progress of lead zirconate-based antiferroelectric materials. *Prog in Materials Science* 2014, **63**: 1-57.

[6] Nie H, Yu Y, Liu Y, *et al*. Enhanced shock performance by disperse porous structure: A case study in PZT 95/5 ferroelectric ceramics. *J Am Ceram Soc* 2017, **100**: 5693-5699.

[7] Xu Z, Feng Y, Zheng S, *et al*. Phase transition and dielectric properties of La-doped $Pb(Zr,Sn,Ti)O_3$ antiferroelectric ceramics under hydrostatic pressure and temperature. *J Appl Phys* 2002, **92**: 2663-2667.

[8] Tan X, Frederick J, Ma C, *et al*. Electric-field-induced antiferroelectric to ferroelectric phase transition in mechanically confined $Pb_{0.99}Nb_{0.02}[(Zr_{0.57}Sn_{0.43})_{0.94}Ti_{0.06}]_{0.98}O_3$. *Phys Rev B* 2010, **81**: 014103.

[9] Kalem V, Çam İ, Timuçin M. Dielectric and piezoelectric properties of PZT ceramics doped with strontium and lanthanum. *Ceram Int* 2011, **37**: 1265-1275.

[10] Zhuo F, Li Q, Gao J, *et al*. Structural phase transition, depolarization and enhanced pyroelectric properties of $(Pb_{1-1.5x}La_x)(Zr_{0.66}Sn_{0.23}Ti_{0.11})O_3$ solid solution. *J Mater Chem C* 2016, **4**: 7110-7118.

[11] Siddiqui M, Mohamed J J, Ahmad Z A. Piezoelectric and dielectric properties of $Pb_{0.93}La_{0.02}Sr_{0.05}(Zr_{0.52}Ti_{0.48})O_3$ ceramics doped with Li_2CO_3 at low sintering temperature. *Ceram Int* 2017, **43**: 2644-2649.

[12] Zeng J, Zhao K, Shi X, *et al*. Large strain induced by the alignment of defect dipoles in (Bi^{3+}, Fe^{3+}) co-doped Pb (Zr, Ti) O_3 ceramics. *Scripta Mater* 2018, **142**: 20-22.

[13] Avdeev M, Jorgensen J D, Short S, *et al*. Pressure-induced ferroelectric to antiferroelectric phase transition in $Pb_{0.99}(Zr_{0.95}Ti_{0.05})_{0.98}Nb_{0.02}O_3$. *Phys Rev B* 2006, **73**: 149902.

[14] Xu Z, Zhai J, Chan W-H, *et al*. Phase transformation and electric field tunable pyroelectric behavior of $Pb(Nb,Zr,Sn,Ti)O_3$ and $(Pb,La)(Zr,Sn,Ti)O_3$ antiferroelectric thin films. *Appl Phys Lett* 2006, **88**: 132908.

[15] Pan W Y, Dam C Q, Zhang Q M, *et al*. Large displacement transducers based on electric field forced phase transitions in the tetragonal $(Pb_{0.97}La_{0.02})$ $(Ti,Zr,Sn)O_3$ family of ceramics. *J Appl Phys* 1989, **66**: 6014-6023.

[16] Jo H R, Lynch C S. Effect of composition on the pressure-driven ferroelectric to antiferroelectric phase transformation behavior of $(Pb_{0.97}La_{0.02})(Zr_{1-x-y}Sn_xTi_y)O_3$ ceramics. *J Appl Phys* 2014, **116**: 074107.

[17] Schmidt N. Coercive force and 90 domain wall motion in ferroelectric PLZT ceramics with square hysteresis loops. *Ferroelectrics* 1981, **31**: 105-111.

[18] Xi Y, Zhili C, Cross L E. Polarization and depolarization behavior of hot pressed lead lanthanum zirconate titanate ceramics. *J Appl Phys* 1983, **54**: 3399-3403.

[19] Hyu-Bum Park C Y P, Young-Sik Hong, Keon Kim, *et al*. Structural and dielectric properties of PLZT ceramics modified with lanthanide ions. *J Am Ceram Society* 1999, **82**: 94-102.

[20] Hu Z, Ma B, Liu S, *et al*. Relaxor behavior and energy storage performance of ferroelectric PLZT thin films with different Zr/Ti ratios. *Ceram Int* 2014, **40**: 557-562.

[21] Zhang G, Chen Z, Fan B, *et al*. Large enhancement of the electrocaloric effect in PLZT ceramics prepared by hot-pressing. *APL Mater* 2016, **4**: 064103.

[22] Liu Y, Ling Z, Zhuo Z. High piezoelectricity of PLZT ceramics with strong frequency-dielectric dispersion below depolarization temperature. *J Alloys Compd* 2017, **727**: 925-930.

[23] Dai X, Viehland D. Effects of lanthanum modification on the antiferroelectric-ferroelectric stability of high zirconium-content lead zirconate titanate. *J Appl Phys* 1994, **76**: 3701-3709.

[24] Kumar A, Prasad V V B, Raju K C J, *et al*. Lanthanum induced diffuse phase transition in high energy mechanochemically processed and poled PLZT 8/60/40 ceramics. *J Alloys Compd* 2016, **654**: 95-102.

[25] Fan L, Chen J, Ren Y, *et al*. Unique piezoelectric properties of the monoclinic phase in $Pb(Zr,Ti)O_3$ ceramics: large lattice strain and negligible domain switching. *Phys Rev Lett* 2016, **116**: 027601.

[26] Ciuchi I V, Mitoseriu L, Galassi C, *et al*. Antiferroelectric to ferroelectric crossover and energy storage properties of $(Pb_{1-x}La_x)(Zr_{0.90}Ti_{0.10})_{1-x/4}O_3$ ($0.02 \leq x \leq 0.04$) ceramics. *J Am Ceram Soc* 2016, **99**: 2382-2387.

[27] Qiao P, Zhang Y, Chen X, *et al*. Enhancing pyroelectric properties in $(Pb_{1-1.5x}La_x)(Zr_{0.86}Ti_{0.14})O_3$ ceramics through composition modulated phase transition. *Ceram Int* 2019, **45**: 7114-7119.

[28] Kumar A, Kalyani A K, Ranjan R, *et al*. Evidence of monoclinic phase and its variation with temperature at morphotropic phase boundary of PLZT ceramics. *J Alloys Compd* 2020, **816**: 152613.

[29] Liu Z, Ren W, Nie H, *et al*. Pressure driven depolarization behavior of Bi0.5Na0.5TiO3 based lead-free ceramics. *Appl Phys Lett* 2017, **110**: 212901.

[30] Yang P, Payne D A. The effect of external field symmetry on the antiferroelectric-ferroelectric phase transformation. *J Appl Phys* 1996, **80**: 4001-4005.

[31] Bao Y, Zhou M, Yan S, *et al*. Novel complex B-site lead oxide antiferroelectric system developed by compositional design for dielectric energy storage. *J Eur Ceram Soc* 2019, **39**: 4785-4793.

[32] Ishchuk V M, Matveev S V, Sobolev V L. Two-phase (ferroelectric and antiferroelectric) nuclei and diffuse phase transition in the vicinity of the ferroelectric-antiferroelectric-paraelectric triple point. *Appl Phys Lett* 2001, **79**: 2949-2951.

[33] Liu P, Yao X. Dielectric properties and phase transitions of $(Pb_{0.87}La_{0.02}Ba_{0.1})(Zr_{0.6}Sn_{0.4-x}Ti_x)O_3$ ceramics with compositions near AFE/RFE phase boundary. *Solid State Commun* 2004, **132**: 809-813.

[34] Schmidt N A. Coercive force and 90° domain wall motion in ferroelectric PLZT ceramics with square hysteresis loops. *Ferroelectrics* 2011, **31**: 105-111.

[35] Zhai J, Li X, Chen H. Effect of the orientation on the ferroelectric–antiferroelectric behavior of sol–gel deposited (Pb,Nb)(Zr,Sn,Ti)O_3 thin films. *Thin Solid Films* 2004, **446**: 200-204.

[36] Peng P, Nie H, Cheng G, et al. Thermal-induced structural transition and depolarization behavior in $(Bi_{0.5}Na_{0.5})TiO_3$-$BiAlO_3$ ceramics. *J Appl Phys* 2018, **123**: 114102.

Figures

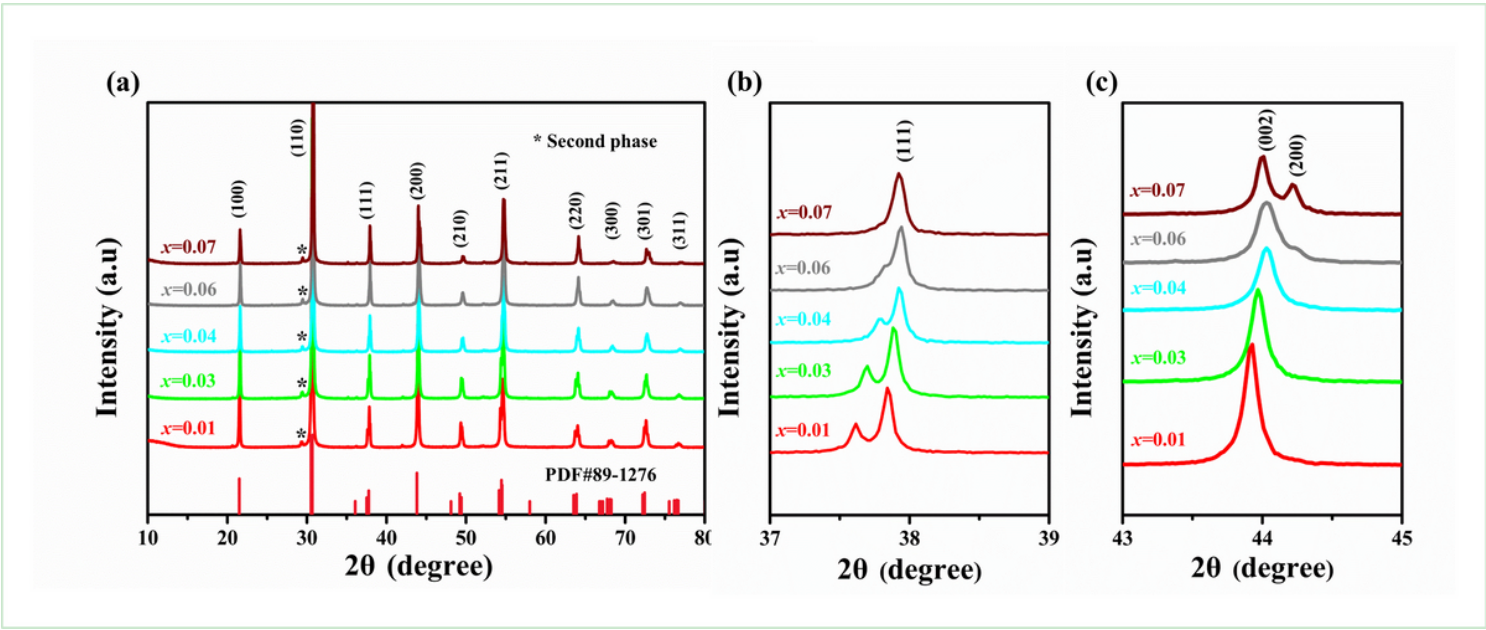

Figure 1

X-ray diffraction patterns of PLZT ceramics with x = 0.01, 0.03, 0.04, 0.06, 0.07 in the range of (a) 10-80°, (b) 37-39°, (c) 43-45°.

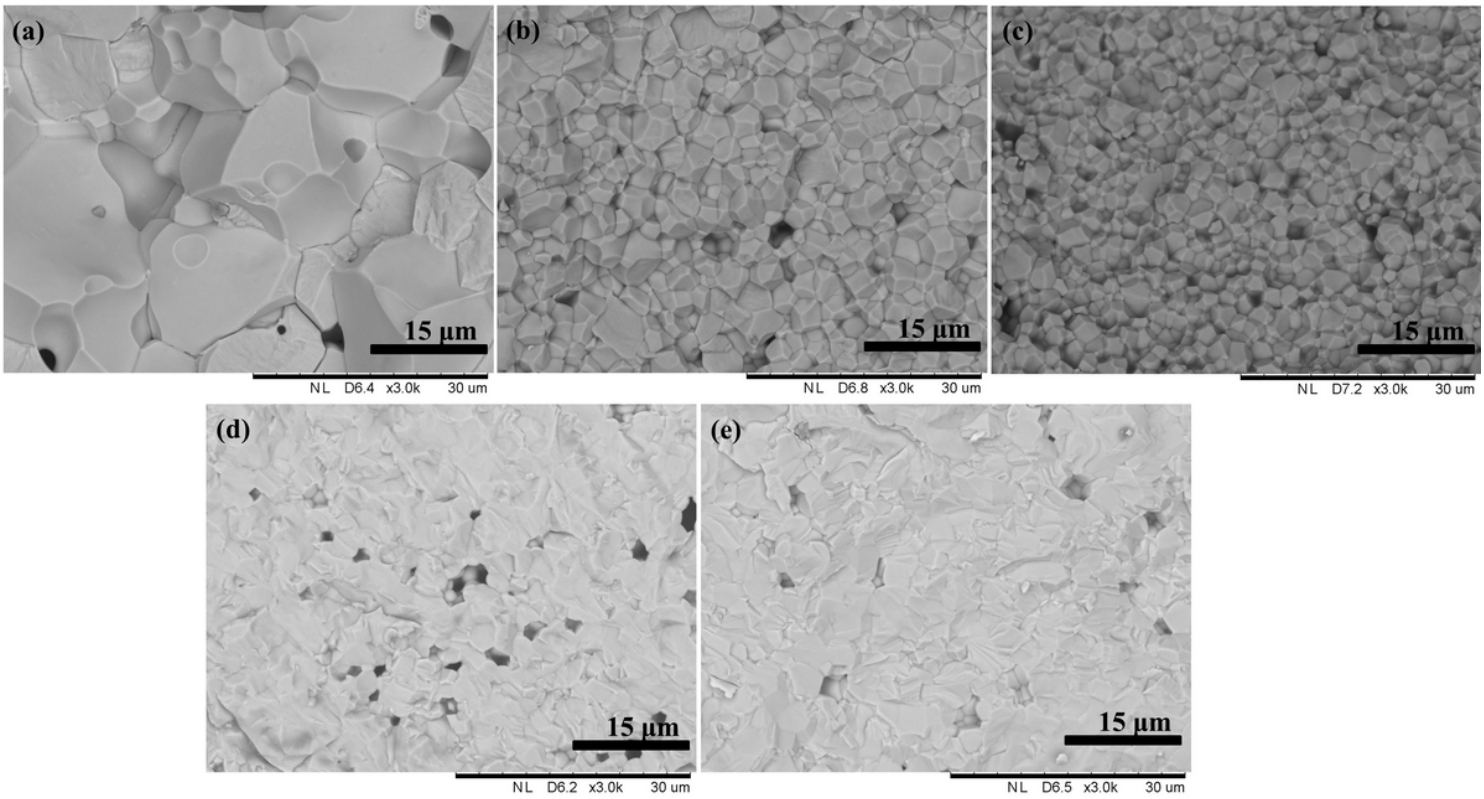

Figure 2

Cross-sectional SEM microstructure of the PLZT ceramics with different La contents: (a) x = 0.01, (b) x = 0.03, (c) x = 0.04, (d) x = 0.06, (e) x = 0.07.

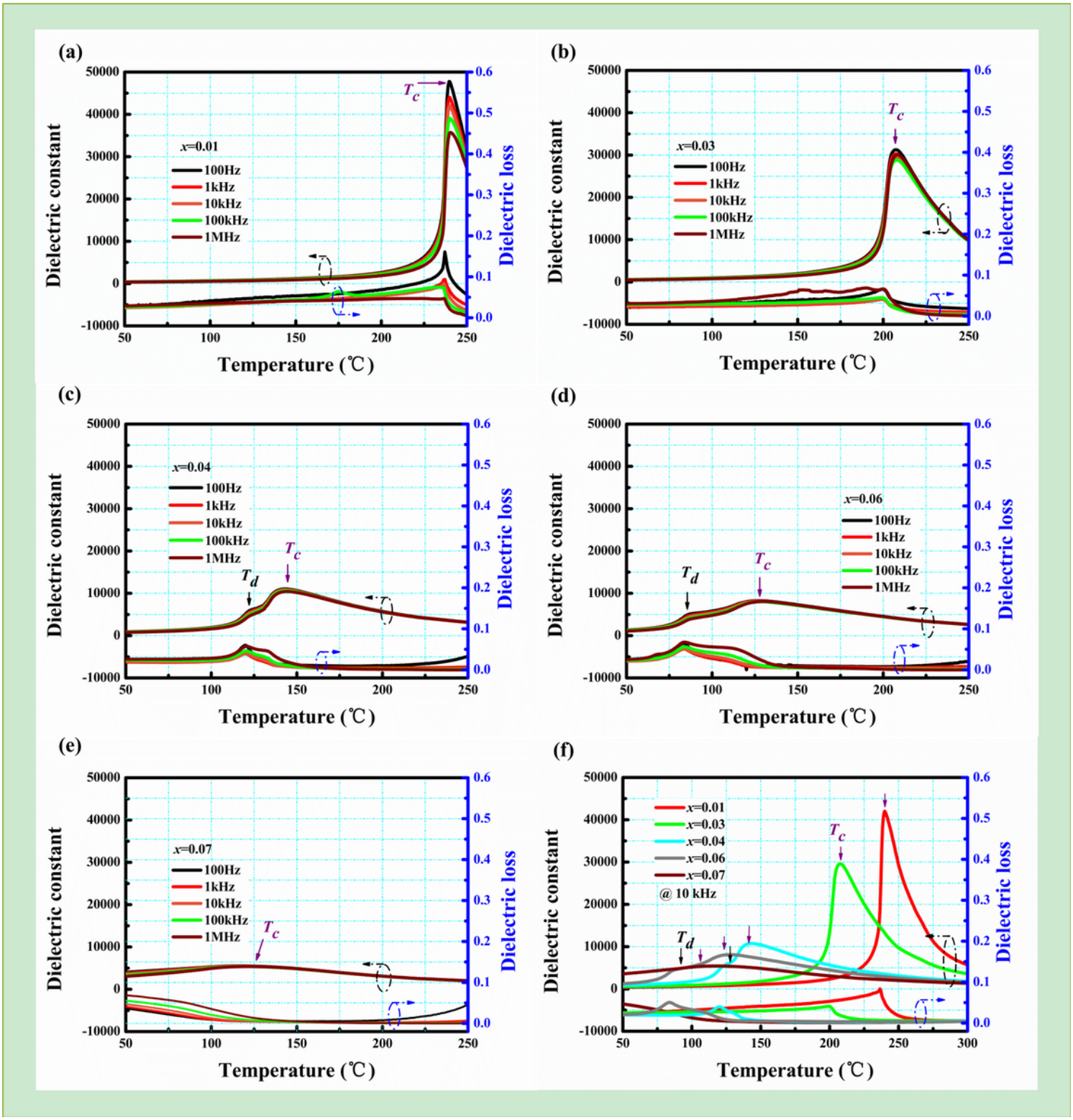

Figure 3

Temperature-dependent relative dielectric constant (ε_r) and dielectric loss (tanδ) from room temperature to 350 °C for poled PLZT ceramics of (a) x = 0.01, (b) x = 0.03, (c) x = 0.04, (d) x = 0.06, (e) x = 0.07 at different frequencies. (f) Temperature-dependent relative dielectric constant (ε_r) and dielectric loss (tanδ) from room temperature to 350 °C for poled PLZT ceramics of (a) x = 0.01, (b) x = 0.03, (c) x = 0.04, (d) x = 0.06, (e) x = 0.07 at 10 kHz

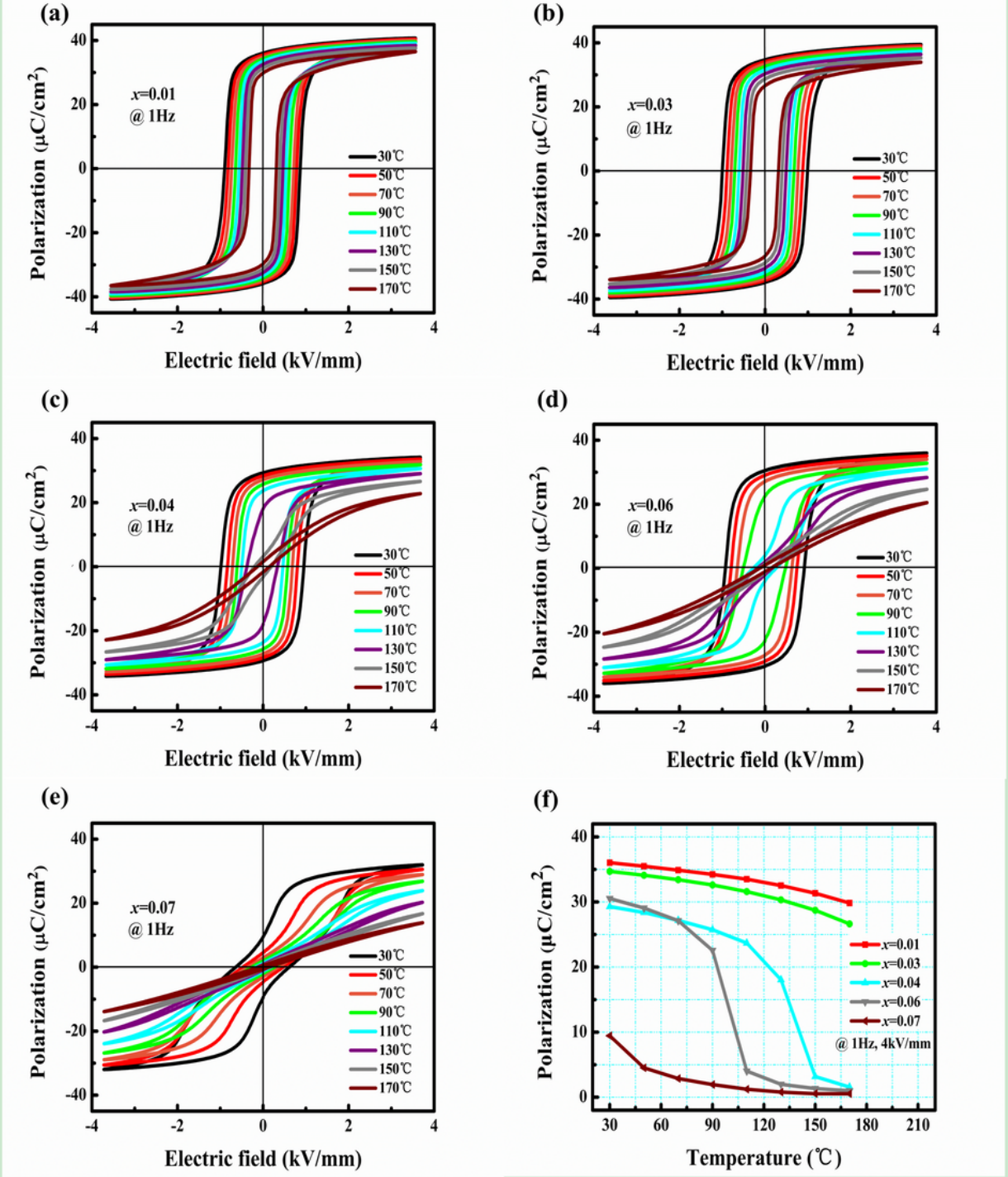

Figure 4

Temperature-dependent P-E hysteresis loops of PLZT(x) under electric field of 4.0kV/mm (1 Hz), (f) Pr of PLZT(x) ceramics tested at different temperature under electric field of 4kV/mm (1 Hz)

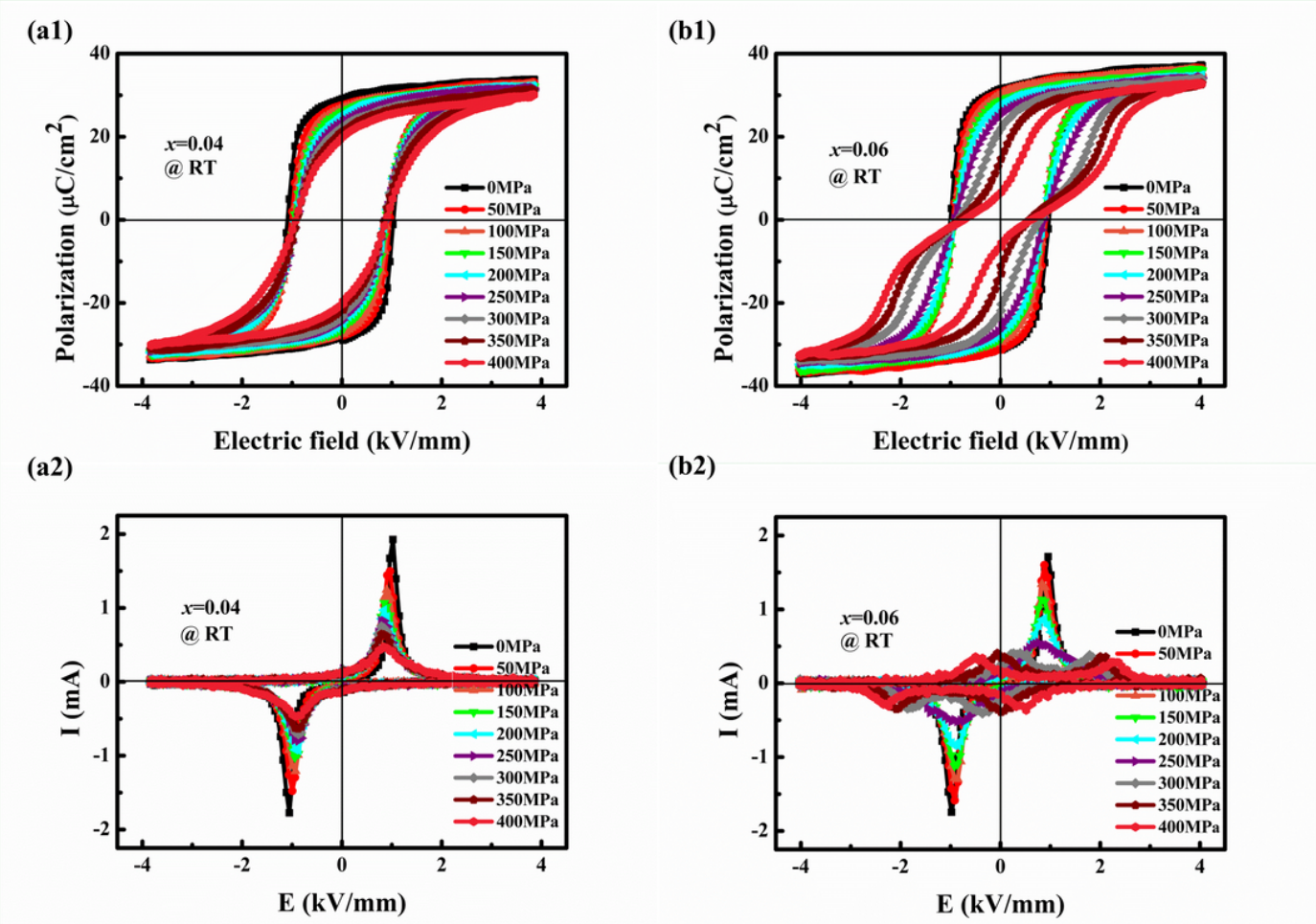

Figure 5

P-E hysteresis loops (a1, b1) and current-field (I-E) curve (a2, b2) of polarized PLZT(x = 0.04, 0.06) ceramics at electric field of 4 kV/mm and under the hydrostatic pressure increasing from 0 MPa to 400 MPa

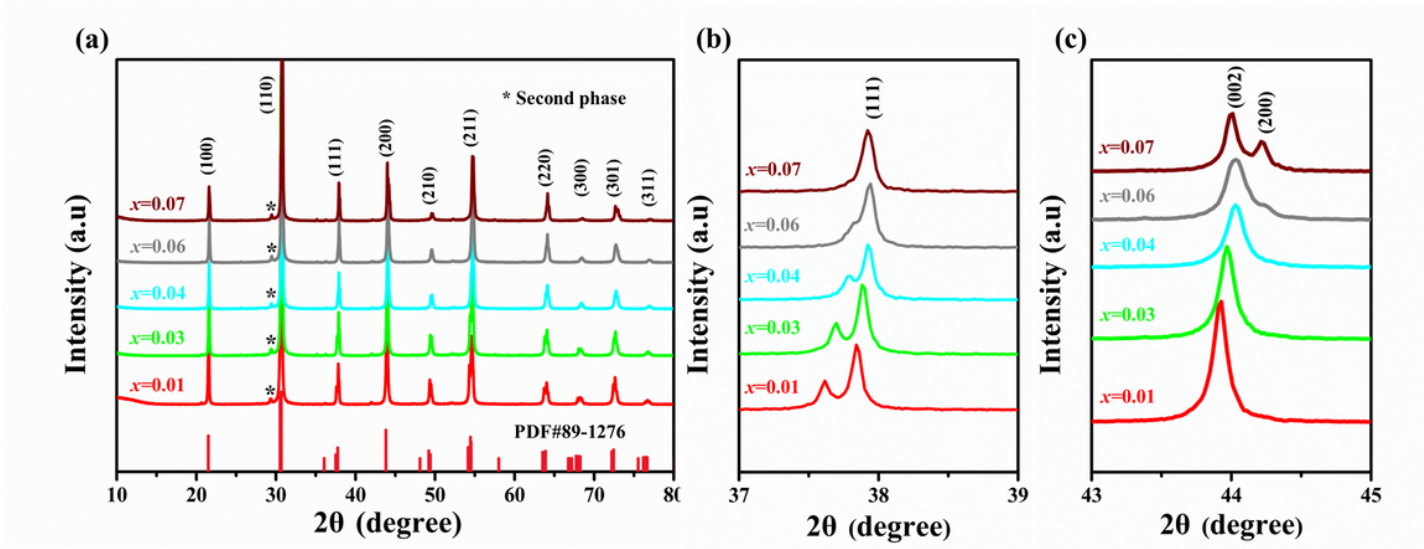

Figure 6

(a) The remnant polarization of PLZT (x = 0.04, 0.06) as function of hydrostatic pressure; (b) Phase diagram for poled (Pb1-1.5xLax)(Zr0.8Ti0.2)O3 ceramics of x = 0.01-0.07.

Supplementary Files

This is a list of supplementary files associated with this preprint. Click to download.

- Equation1.pdf